Antoniadis, I. and Chronopoulos, D. and Spitas, V. and Koulocheris, D. (2015) Hyper-damping properties of a stiff and stable linear oscillator with a negative stiffness element. Journal of Sound and Vibration, 346 . pp. 37-52. ISSN 0022-460X

Hyper-damping properties of a stiff and stable linear oscillator with a negative stiffness element

I. Antoniadis[a], D. Chronopoulos[b], V. Spitas[a], D. Koulocheris[a]

[a]*Machine Design and Control Systems Section, School of Mechanical Engineering, National Technical University of Athens, Greece*
[b]*Division of Materials, Mechanics and Structures, University Park, The University of Nottingham, NG7 2RD, UK*

Abstract

A simple, stiff, statically and dynamically stable linear oscillator incorporating a negative stiffness element is used as a template to provide a generic theoretical basis for a novel vibration damping and isolation concept. This oscillator is designed to present the same overall static stiffness, the same mass and to use the same damping element as a reference classical linear SDoF oscillator. Thus, no increase of the structure mass or the viscous damping is needed, as in the case of a traditional linear isolator, no decrease of the overall structure stiffness is required as in the case of 'zero-stiffness' oscillators with embedded negative stiffness elements. The difference from these two templates consists entirely in the proper redistribution and reallocation of the stiffness and the damping elements of the system. Once such an oscillator is optimally designed, it is shown to exhibit an extraordinary apparent damping ratio, which is even several orders of magnitude higher than that of the original SDoF system, especially in cases where the original damping of the SDoF system is extremely low. This extraordinary damping behavior is a result of the phase difference between the positive and the negative stiffness elastic forces, which is in turn a consequence of the proper redistribution of the stiffness and the damping elements. This fact ensures that an adequate level of elastic forces exists throughout the entire frequency range, able to counteract the inertial and the excitation forces. Consequently, a resonance phenomenon, which is inherent in the original linear SDoF system, cannot emerge in the proposed oscillator. The optimal parameter selection for the design of the negative stiffness oscillator is discussed. To further exhibit the advantages that such a design can generate, the suggested oscillator is implemented within a periodic acoustic metamaterial structure, inducing a radical increase in the damping of the propagating acoustic waves. The concept may find numerous technological applications, either as traditional vibration isolators, or within advanced composite materials and metamaterials.

Keywords: Damping, Vibration isolation, Viscoelasticity, Negative stiffness, Metamaterial

1. Introduction

Damping is an influence that has the effect of reducing, restricting or preventing the oscillations of a dynamic system. The current engineering and physical perception is that damping is produced by mechanisms responsible to dissipate the energy stored in the oscillating system. Such mechanisms include passive means like friction, hysteresis, drag, hydraulic and electrical resistance, or active means, often based on smart materials.

Concerning the design of materials or continuous structures, the most frequently used highly dissipative damping materials are characterized by moderate to low stiffness, which renders them unsuitable for demanding load carrying applications, viscoelastic materials being the most prominent example [1, 2]. Such a limitation is quite restrictive in applications requiring high stiffness and often low weight, the most characteristic examples being in the aerospace and automotive sectors [3].

The established approach to address this challenge is the compromise of designing composite materials with multiple phases or layers of different constituents, exhibiting either high stiffness or high damping [4]. The most important recent research trend towards this direction, is the design of specific classes of periodic structures, known as metamaterials [5, 6]. Among the most fascinating properties of such natural or artificial structures are their attenuation effects. When the frequency of the waves falls into their 'blind' zone, the propagation of waves is forbidden in any direction, forming thus a 'band-gap'.

However, existing metamaterial types fail to provide effective broadband vibration attenuation in the middle to low sub kHz frequency range. Phononic metamaterials, based on Bragg scattering are targeted to high frequency ranges, as for e.g. to the ultrasonic range, since the dimensions of the lattices they require are proportional to the wavelengths of the transmitted wave [7], and are thus prohibitive to the frequency range mentioned. Acoustic metamaterials [8], intended to cover this disadvantage, require additional masses, which renders them also inappropriate for a broad class of applications, due to the additional weight they induce. Even the recent concept of 'metadamping' [9] requires acoustic metamaterials in order to be effectively performed.

Parallel, other periodic cellular structures have been reported to present increased damping properties, while they simultane-

Email addresses: antogian@central.ntua.gr (I. Antoniadis), Dimitrios.Chronopoulos@nottingham.ac.uk (D. Chronopoulos)

ously incorporate stiffness elements inherently capable to combine positive and negative stiffness behavior [10, 11, 12]. Some underlying physical mechanisms, such as microbuckling [13] or slip- stick phenomena [14] have been considered to contribute to the enhanced dynamic properties of such structures.

A quite interesting possibility towards achieving significant damping has been demonstrated to exist in materials comprising a negative stiffness phase [4], not only at a material level [15], but also at macroscopic devices [16]. Quite interestingly, such a behavior is combined with high stiffness properties. A theoretical analysis has been performed for the analysis of the static and dynamic stability composites, incorporating negative stiffness elements [17].

A quite similar approach exists for the design of engineering structures where vibration damping is achieved by the use of discrete macroscopic elements, such as springs and dampers. It should be noted that the concept of introducing negative stiffness elements (or 'anti-springs') for vibration isolation has a long history, being first introduced in the pioneering publication of Molyneaux [18] as well as in the milestone developments of Platus [19]. A rich variety of designs have been proposed for the realization of negative spring configurations, incorporating various structural elements such as post-buckled beams, plates, shells and precompressed springs, arranged in appropriate geometrical configurations. Some interesting designs are described in [20, 21, 22, 23, 24]. The central concept of these approaches is to significantly reduce the stiffness of the isolator and consequently of the natural frequency of the system even at almost zero levels [25]. In this way, the transmissibility of the system for all operating frequencies above the natural frequency is reduced, resulting to enhanced vibration isolation. An initial comprehensive review of such designs can be found in [26]. Since then, numerous other applications have been reported in a diversity of engineering domains, such as automotive suspensions [27, 28, 29] or seismic isolation [24, 30, 31]. From the fundamental design point of view, many interesting improvements have been proposed, based on the non-linear properties of the elastic force of such designs [32, 33, 34, 35, 36]. However, all these designs suffer from their fundamental requirement for a drastic reduction of the stiffness of the structure almost to negligible levels, limiting thus the static load capacity of such structures.

This paper proposes an approach on how to optimally design a simple linear oscillator incorporating a negative stiffness element, which can exhibit extraordinary-damping properties, without presenting the drawbacks of the traditional linear oscillator, or of the 'zero-stiffness' designs. Section 2 presents the basic dynamic analysis and design concept of such an oscillator. The oscillator is designed to present the same overall (static) stiffness, as a traditional reference original oscillator, in order to overcome the inherent disadvantage of the known negative stiffness oscillators in requiring stiffness reduction. Moreover, it does not require any increase in the mass or the viscous damping of the original oscillator in order to increase the vibration isolation properties, as it is the case of the traditional linear vibration isolators. However, it differs both from the the original SDoF oscillator as well as from the known negative stiffness oscillators by appropriately redistributing the individual stiffness elements and by reallocating the damping. Despite the fact that the proposed oscillator incorporates a negative stiffness element, it is designed to be both statically and dynamically stable.

Section 3 proceeds to a parametric analysis and optimal design of the oscillator. Once such a system is designed according to the approach proposed, it is shown to exhibit an extraordinary damping behavior, with an apparent damping ratio to be even several orders of magnitude higher than that of the original system, especially in the cases where the original damping of the system is extremely low. Although the elastic members of the proposed system need to be redesigned with a stiffness higher than that of the original system, such an increase is within reasonable engineering limits. Results in both the frequency and the time domain are exhibited and discussed on the response of the suggested oscillator.

Further analysis in Section 4 indicates that the physical mechanism responsible for the vibration attenuation is significantly different than that of the original SDoF oscillator. It is exhibited that the exceptional damping behaviour of the proposed oscillator, is a result of the phase difference between the positive and the negative stiffness elastic forces. Moreover, analysis of the peak level of the damper force in the proposed oscillator indicates that its level is significantly lower than that of the peak level of the traditional SDoF system, despite the extraordinary damping behavior introduced. These mechanisms are also confirmed by conducting a transient energy flow analysis within the modified oscillator.

Section 5 proceeds to initial demonstrations on how such oscillators can be arranged in appropriate periodic acoustic metamaterial lattices or periodic composite structures, enhancing both their damping properties, as well as their band-gap behaviour.

2. Design approach for a stiff, statically and dynamically stable oscillator incorporating a negative stiffness element

2.1. Dynamic analysis

The design of the considered oscillator with the inclusion of a negative stiffness element κ_c is introduced in Fig. 1, in distinction to a classical linear SDoF oscillator, as well as to the known negative stiffness designs. Moreover, Fig. 2 presents a conceptual design of a vibration isolator designed according to the proposed oscillator, in distinction to the known negative stiffness oscillators.

The static stiffness $\kappa_{st,m}$ of the modified oscillator can be expressed as

$$\kappa_{st,m} = \kappa_s + \frac{\kappa_e \kappa_c}{\kappa_e + \kappa_c} \tag{1}$$

[Figure 1 about here.]

In order to ensure that the damping and isolation properties of the oscillator considered do not result to any adverse effect to the overall stiffness and load carrying capacity of the structure, the static stiffness of the modified system will be set equal to

κ_0 throughout this work, thus $\kappa_0 = \kappa_{st,m}$. The two systems also comprise the same damping element of coefficient η.

[Figure 2 about here.]

The equations of motion for the DoF x, y of the modified system illustrated in Fig. 1 can be written as

$$m\ddot{x} + \eta(\dot{x} - \dot{y}) + \kappa_s x + \kappa_e(x - y) = f \tag{2a}$$
$$\eta(\dot{x} - \dot{y}) + \kappa_e(x - y) - \kappa_c y = 0 \tag{2b}$$

or by combining Eqs. 2a, 2b

$$m\ddot{x} + k_s x + k_c y = f \tag{3}$$

with f being the external excitation applied to the 'apparent' DoF x. It is evident that an internal DoF hereby named y arises for the modified system in order to describe the displacement of the κ_c stiffness element. The system can therefore be characterized as an oscillator with one apparent and one internal (hidden) DoF, taking into account Eq. 2b.

With the application of a Laplace transform the above system can be expressed as

$$s^2 mX + s\eta(X - Y) + \kappa_s X + \kappa_e(X - Y) = F \tag{4a}$$
$$s\eta(X - Y) + \kappa_e(X - Y) - \kappa_c Y = 0 \tag{4b}$$

Rearranging the terms in Eqs. 4a, 4b gives

$$s^2 mX + s\eta X + (\kappa_s + \kappa_e)X - (s\eta + \kappa_e)Y = F \tag{5a}$$
$$Y = \frac{s\eta + \kappa_e}{s\eta + (\kappa_e + \kappa_c)}X \tag{5b}$$

and by inserting Eq. 5b in 5a

$$[s^2 m + s\eta + (\kappa_s + \kappa_e)]X - \frac{(s\eta + \kappa_e)^2}{[s\eta + (\kappa_e + \kappa_c)]}X = F \tag{6}$$

In order to bring the transfer function of the system X/F to a convenient form from which the poles of the system can be computed Eq. 6 is written as

$$\frac{c_1 s^3 + c_2 s^2 + c_3 s + c_4}{[s\eta + (\kappa_e + \kappa_c)]}X = F \tag{7}$$

with

$$c_1 = m\eta \tag{8a}$$
$$c_2 = m(\kappa_e + \kappa_c) \tag{8b}$$
$$c_3 = \eta(\kappa_s + \kappa_c) \tag{8c}$$
$$c_4 = \kappa_s(\kappa_e + \kappa_c) + \kappa_e\kappa_c \tag{8d}$$

Therefore

$$X = \frac{[s\eta + (\kappa_e + \kappa_c)]}{c_1 s^3 + c_2 s^2 + c_3 s + c_4}F \tag{9}$$

with $c_1 s^3 + c_2 s^2 + c_3 s + c_4$ being the characteristic equation of the modified system. The system will therefore have one real and two complex poles in which case its transfer function can also be expressed as

$$X = \frac{[s\eta + (\kappa_e + \kappa_c)]}{m\eta(s + \rho)(s^2 + 2\zeta_n\omega_n s + \omega_n^2)}F \tag{10}$$

with ρ the real pole of the characteristic equation, ζ_n the new damping ratio of the modified system and ω_n its new resonant frequency. At this point it should be noted that the mass m_y associated with the internal DoF y has been safely omitted assuming that $m \gg m_y$. Accounting for a non-zero mass for the y DoF would induce a fourth order characteristic equation for Eq. 9 and therefore an additional condition to be satisfied for the stability of the oscillator. A second mass would also induce a second resonance for the two DoF system, which would however be frequency-wise much higher than the fundamental resonance. Comparing the denominators in Eqs. 9, 10 it can be observed that

$$\rho + 2\zeta_n\omega_n = \xi = \frac{\kappa_e + \kappa_c}{\eta} \tag{11a}$$
$$2\rho\zeta_n\omega_n + \omega_n^2 = \frac{\kappa_s + \kappa_c}{m} \tag{11b}$$
$$\rho\omega_n^2 = \xi\omega_0^2 \tag{11c}$$

In order for the system to be dynamically stable the following conditions should be satisfied

$$\rho \geq 0 \tag{12a}$$
$$\zeta_n \geq 0 \tag{12b}$$
$$\omega_n \geq 0 \tag{12c}$$

Eqs. 11, 12 define the basic requirements and concepts for the design of the proposed oscillator. First, as a direct consequence of Eq. 12, it results that

$$\xi > 0 \Leftrightarrow \kappa_e + \kappa_c > 0 \tag{13}$$

Furthermore, in order that the new oscillator exhibits maximum damping, the term $\zeta_n\omega_n$ should be maximum. Therefore, for a constant ξ, and in view of Eq. 11a, ρ should be close to zero. In view of Eq. 11c, this in turn implies that ω_0 and κ_0 should be positive but close to zero. That is, the system should be designed close to the neutral stability point

$$\kappa_0 = \kappa_s + \frac{\kappa_e\kappa_c}{\kappa_e + \kappa_c} = 0 \tag{14}$$

2.2. Suggested engineering design

In order for the modified system to be equivalent to the SDoF oscillator the following relation is true for the static stiffnesses of the two configurations

$$\kappa_0 = \kappa_s + \frac{\kappa_e\kappa_c}{\kappa_e + \kappa_c} \tag{15}$$

The right part of Eq. 15 contains three unknown stiffness terms. In order to proceed to a concrete design of the modified system two additional relations are sought for κ_s, κ_c and κ_e. The first one will be assuming a linear relation between κ_s and κ_0 as

$$\kappa_s = \alpha\kappa_0 \tag{16}$$

with $\alpha \geq 1$. It is evident that for α=1 the system will converge to the SDoF oscillator behaviour and that for greater values of α the negative term $\frac{\kappa_e\kappa_c}{\kappa_e+\kappa_c}$ will be responsible for reestablishing Eq. 15. The second relation is derived by considering that an engineering safety margin ε should exist for the selection of κ_c, prohibiting it to reach its limit value, that would result to a statically unstable structure:

$$\kappa_s + \frac{(1+\varepsilon)\kappa_c\kappa_e}{(1+\varepsilon)\kappa_c + \kappa_e} = 0 \tag{17}$$

For the system to be statically stable it is assumed that $\varepsilon > 0$. Solving the system of Eqs. 15-17 the design values for the stiffnesses are obtained as

$$\kappa_e = \kappa_0 \frac{\varepsilon\alpha(\alpha-1)}{1+\varepsilon-\alpha\varepsilon} \tag{18a}$$

$$\kappa_c = -\kappa_0 \frac{\varepsilon\alpha(\alpha-1)}{1+\varepsilon} \tag{18b}$$

From Eq. 18 and for $\alpha > 1$ it can be observed that

$$\kappa_e > 0 \Leftrightarrow 1+\varepsilon > \alpha\varepsilon \Leftrightarrow \alpha < \frac{1+\varepsilon}{\varepsilon} \tag{19a}$$

$$\kappa_e + \kappa_c > 0 \tag{19b}$$

are implied design limitations of the system. It is interesting to notice that Eqs. 18,19 fully satisfy the necessary and sufficient conditions for static stability, independently derived in [17].

3. Optimal parameter selection and analysis of the response of the proposed oscillator

It would be strongly beneficial for the designer to directly derive the design parameters for the stiffnesses κ_s, κ_e, κ_c as a function of κ_0, ω_0, m, η and the desired values of ζ_n and ω_n. This can indeed be done by introducing Eqs. 17,18 in Eq. 11 and subsequently solve for ζ_n and ω_n as a function of the design variables α, ε and the characteristics of the SDoF oscillator κ_0, η, m. Due to the complexity of the resulting equations however this optimisation procedure is outside the scope of this work.

Eq. 10 implies that the new considered oscillator is dynamically equivalent to a SDoF oscillator with a new apparent damping ratio ζ_n and natural frequency ω_n, since the value of ρ is always positive. Moreover, Eqs. 18, 19 imply that the absolute values of the stiffness elements κ_s, κ_e, κ_c are greater than the stiffness κ_0 of the original oscillator.

Consequently, a parametric analysis is performed to examine the effect of the freely selectable parameters α and ε on the resulting values of the stiffness elements, as well as on the apparent dynamic parameters ω_n and ζ_n. The analysis is performed for a reference initial linear oscillator with non-dimensional value of ω_0= 2π rad/sec, ζ_0=0.01 and κ_0= 1 N/m.

3.1. Selection of the stiffness design values

The approach involves the examination of the effect of the design parameters α, η and ε on the stiffness values κ_s, κ_e and κ_c of the oscillator considered.

The results on the dependence of κ_e on α are presented in Fig. 3.

[Figure 3 about here.]

It is observed that increasing ε will demand a higher stiffness for κ_e in order for a certain static stiffness κ_0 to be retained. This difference is as significant as 500% when comparing the values between ε=1.5%, ε=10%, for α=10. It is also shown that κ_e increases monotonically with κ_s.

[Figure 4 about here.]

In Fig. 4 similar results are exhibited, this time for stiffness κ_c. Again it is observed that in order for a certain static stiffness κ_0 to be retained a more significant negative stiffness will be demanded for κ_c. It can therefore generally be concluded that considering the design of the oscillator it is more practical to choose a low ε values.

3.2. Parametric damping analysis of the proposed oscillator

One of the most important design objectives for the oscillator is maximizing its damping characteristics. The damping ratio ζ_n of the modified system can be calculated as a function of the poles of the characteristic equation of the system. In Fig. 5 the values of ζ_n as a function of α and for various ε values are presented. The results are given as the ratio of ζ_n to the damping ratio of the SDoF system

$$\zeta_0 = \frac{\eta}{2\sqrt{m\kappa_0}} \tag{20}$$

It is shown that for every ε value an optimal α value exists for maximizing ζ_n. The lower the ε value, the greater the optimal value of the attained ζ_n. For higher α values, ζ_n converges to the statically equivalent SDoF system. It can also be concluded that increasing ε will significantly decrease the optimal α.

[Figure 5 about here.]

A similar graph exhibiting the attained damping ratio ζ_n for various values of the damping coefficient η of the dashpot is shown in Fig. 6. Again an optimal α value seems to exist for any η in order to maximize the damping ratio of the system. As expected, increasing η increases ζ_n; however this increase is not linear. Taking a look at the maximum ζ_n values it is observed that increasing η by a factor of 100 will only increase the maximum ζ_n by a factor of 4. Comparing the maximum ζ_n values to ζ_0 it is observed that for ζ_0 = 1% the damping ratio is amplified by a factor of 18, while for ζ_0 = 0.1% the damping ratio is increased by a factor of 100. It can therefore be concluded that an impressive improvement of the damping capabilities takes place for the modified system; this improvement is greater for lightly damped systems.

[Figure 6 about here.]

3.3. Impact of the design on the natural frequency of the oscillator

It is hereby stressed that the natural frequency ω_n of the modified oscillator is also dependent on α and can be calculated as a function of the poles of the characteristic equation. In Fig. 7 the ratio $\Omega = \omega_n/\omega_0$ is exhibited as a function of α for various ε values. It is observed that decreasing ε increases Ω. This increase becomes more significant when getting closer to the stability limit $\lim \varepsilon \to 0^+$. For greater α values Ω converges to unity and the configuration is deprived of any exceptional damping behavior.

In Fig. 8, Ω is plotted as a function of α for various values of ζ_0. It is shown that a greater η will increase the natural frequency of the modified system. Again, for higher α values Ω converges back to unity.

[Figure 7 about here.]

[Figure 8 about here.]

3.4. Frequency domain response

Using Eq. 7 the frequency response function FRF of the response X can be expressed as

$$\frac{X}{F} = \frac{\mathrm{i}\omega\eta + (\kappa_e + \kappa_c)}{c_1(\mathrm{i}\omega)^3 + c_2(\mathrm{i}\omega)^2 + c_3(\mathrm{i}\omega) + c_4} \tag{21}$$

with the coefficients c_i given by Eq. 8.

Observing Figs. 5-8 it is evident that among others, two design options exist for minimizing the response of the system; the first one being the choice of a value for α that will maximize ζ_n. The second option would be selecting a value for α that would maximize the resonance frequency of the system, in which case the resonance band of the SDoF system would be transformed into a low frequency/ low response regime.

In Figs. 5,7, it can be observed that minimizing ε will result in increased Ω and ζ_n values for the system. It can therefore be assumed that an optimal performance will be attained for $\lim \varepsilon \to 0^+$. In Fig. 9 a low value for ε of 1% is inserted in the calculations. The results show a drastic reduction of the FRF X/F. For an Ω optimal α a maximum reduction of 2100% in the response of the system is observed. The reduction is slightly less impressive for a ζ_n maximizing α parameter. In the high frequency range the responses seems to converge to that of the SDoF system.

[Figure 9 about here.]

3.5. Transient response and impact isolation capacities

The first part of the numerical case studies is dedicated to investigating the time domain response of the system. In order to solve for the time dependent response the system of equations in Eq. 2 will be expressed in a state-space form with

$$x_1 = x \tag{22a}$$
$$x_2 = \dot{x} \tag{22b}$$
$$x_3 = y \tag{22c}$$

Inserting Eq. 2b into 2a and rearranging the terms

$$m\ddot{x} + \kappa_s x + \kappa_c y = f \Leftrightarrow \ddot{x} = (f - \kappa_s x - \kappa_c y)/m \tag{23a}$$
$$\eta\dot{y} = \eta\dot{x} + \kappa_e(x - y) - \kappa_c y \Leftrightarrow \dot{y} = \dot{x} + \frac{\kappa_e}{\eta}(x - y) - \frac{\kappa_c}{\eta}y \tag{23b}$$

Therefore the derivatives can be written as

$$\dot{x_1} = x_2 \tag{24a}$$
$$\dot{x_2} = (f - \kappa_s x_1 - \kappa_c x_3)/m \tag{24b}$$
$$\dot{x_3} = x_2 + \frac{\kappa_e}{\eta}(x_1 - x_3) - \frac{\kappa_c}{\eta}x_3 \tag{24c}$$

The results can eventually be obtained by applying a Runge-Kutta numerical approach. A unitary initial velocity is considered for y simulating thus a vibro-impact situation. The initial displacements are both set to zero. The values κ_0, m and η for the equivalent SDoF system are the same as aforementioned in Sec. 3.

In Fig. 10 the results for the time dependent response of $\dot{x}$, $\dot{y}$ are exhibited. An Ω optimal α value is hereby considered. It can be observed that the values attained by $\dot{y}$ are much greater than the ones for $\dot{x}$ as expected from the Y/X transfer function results presented in Fig. 12. The phase difference in the two curves is also evident.

[Figure 10 about here.]

In Fig. 11 the corresponding results for the time dependent forces applied within the modified system are exhibited. The phase difference between the stiffness forces and the inertial forces can be observed.

[Figure 11 about here.]

4. The physical background of the damping mechanism

4.1. The importance of the emergent phase $\angle Y/X$

In view of Eq. 2, it is evident that if the amplitudes and the phases of X, Y were equal then $\eta(\dot{x} - \dot{y}) = 0$ which means that the damping force and therefore the energy absorbed by the damping mechanism would inevitably be nil. The transfer function Y/X can be deduced by Eq. 5b while the FRF Y/F can be written as

$$\frac{Y}{F} = \frac{\mathrm{i}\omega\eta + \kappa_e}{\mathrm{i}\omega\eta + (\kappa_e + \kappa_c)}X = \frac{\mathrm{i}\omega\eta + \kappa_e}{c_1(\mathrm{i}\omega)^3 + c_2(\mathrm{i}\omega)^2 + c_3(\mathrm{i}\omega) + c_4} \tag{25}$$

In Fig. 12 the transfer function Y/X is shown for a range of α values. In Fig. 13 similar graphs for the phases of transfer functions $\angle X/F$ and $\angle Y/F$ are plotted. For high α values (much greater that the ones in the optimal range) the transfer function Y/X will converge to unity, suggesting that the response will converge towards the one of the original SDoF oscillator.

On the other hand when an optimal design parameter α is selected the transfer function Y/X attains greater values, implying that small displacements of X can induce great internal Y

displacements. Furthermore $\angle X/F$ and $\angle Y/F$ diverge even in the low frequency range with a maximum divergence of approximately 1 radian which is in favour of maximizing ζ_n.

[Figure 12 about here.]

[Figure 13 about here.]

It can generally be concluded that the impressive reduction of the X/F response of the modified system observed in Fig. 9 is underpinned by two factors, with the first one being the amplification of the internal response Y of the system for low responses of X. The second one exhibited in Fig. 13 being the emergence of a phase difference between the FRFs of X/F and Y/F, which increases the time averaged relative velocity $\dot{x}$-$\dot{y}$.

The physical mechanism, responsible for the extraordinary vibration damping is better revealed by the analysis of the forces developed during the operation of the system. The forces can be calculated as

$$F_m = m\ddot{x} \Rightarrow F_{mt} = (\mathrm{i}\omega)mX \tag{26a}$$
$$F_s = k_s x \Rightarrow F_{st} = k_s X \tag{26b}$$
$$F_c = k_c y \Rightarrow F_{ct} = k_c Y \tag{26c}$$
$$F_e = k_e(x-y) \Rightarrow F_{et} = k_e Z \tag{26d}$$
$$F_h = \eta(\dot{x}-\dot{y}) \Rightarrow F_{ht} = (\mathrm{i}\omega)\eta Z \tag{26e}$$

with $Z = X - Y$. In Fig. 14 the resulting real parts of the developed forces are exhibited for the conventional SDoF oscillator. Since the applied external excitation is of unit amplitude, the sum of the real parts of the forces has to be equal to unity for all frequencies. In accordance to the classical theory of the linear SDoF oscillator, the real part of the elastic and inertial forces become zero in the vicinity of the resonance leaving solely the damping force to counteract the external excitation.

The results for the suggested configuration when an optimal α design value is chosen are shown in Fig. 15. The external excitation curve (equal to unity throughout the frequency range) is omitted for the sake of conciseness. It is observed that in the vicinity of the new resonance of the system ω_n the positive stiffness and inertial forces become zero, however in this case it is the the real part of the force provided by the negative stiffness κ_c that contributes to counterbalancing the external excitation. This phenomenon can be attributed to the phase difference $\angle X/F$ described above.

[Figure 14 about here.]

[Figure 15 about here.]

A further interesting result of Figs. 14, 15 is the fact that the peak real part of the damping force of the considered oscillator is significantly less than that of the reference SDoF system, despite the extraordinary damping behaviour.

4.2. Transient energy flow analysis in the proposed oscillator

A transient energy flow analysis is further considered in order to give further insight on how the damping of the oscillator is increased compared to the SDoF system. About the energy flow it is known that

$$\frac{\mathrm{d}E_t}{\mathrm{d}t} + \eta(\dot{x}-\dot{y})^2 = f\dot{x} \tag{27}$$

with E_t the total mechanical energy in the oscillator defined as

$$E_t = E_p + E_m \tag{28a}$$
$$E_m = \frac{1}{2}m\dot{x}^2 \tag{28b}$$

with E_m the total kinetic energy and E_p the total potential energy calculated as

$$E_p = E_s + E_e + E_c \tag{29a}$$
$$E_s = \frac{1}{2}\kappa_s x^2 \tag{29b}$$
$$E_e = \frac{1}{2}\kappa_e(x-y)^2 \tag{29c}$$
$$E_c = \frac{1}{2}\kappa_c y^2 \tag{29d}$$

Further elaboration of equation Eq. 29 leads to

$$\dot{E}_s + \dot{E}_e + \dot{E}_c + \dot{E}_m + \eta(\dot{x}-\dot{y})^2 = f\dot{x} \tag{30a}$$
$$\dot{E}_s = \kappa_s x\dot{x} \tag{30b}$$
$$\dot{E}_e = \kappa_e(x-y)(\dot{x}-\dot{y}) \tag{30c}$$
$$\dot{E}_c = \kappa_c y\dot{y} \tag{30d}$$
$$\dot{E}_m = \kappa_s \dot{x}\ddot{x} \tag{30e}$$

while the corresponding equation for the original reference SDoF oscillator is

$$\dot{E}_{p0} + \dot{E}_{m0} + \eta\dot{x}^2 = f\dot{x} \tag{31a}$$
$$\dot{E}_{p0} = \frac{\mathrm{d}(\kappa_0 x^2/2)}{\mathrm{d}t} = \kappa_0 x\dot{x} \tag{31b}$$
$$\dot{E}_{m0} = \frac{\mathrm{d}(m\dot{x}^2/2)}{\mathrm{d}t} = m\dot{x}\ddot{x} \tag{31c}$$

Fig. 16 depicts the rate of change of the potential energy, of the kinetic energy and of the power dissipated in the damper for the equivalent original linear oscillator. A phase difference of 180^o exists between the rate of change of the total potential energy and the kinetic energy. Thus, in view of Eq. 31, a minimal amount of power is absorbed in the damper.

[Figure 16 about here.]

Fig. 17 depicts the rate of change of the potential energies of the oscillator having negative stiffness inclusions. As it can be observed, a phase difference exists between the rate of change of the potential energy of the positive stiffness elements, as a consequence of the phase difference between x and y. Moreover, the negative stiffness element results to a phase difference of almost 180^o between the rate of change of the potential energy of the negative stiffness spring and the rate of change of

the potential energies of the positive stiffness springs. This indicates that the role of the negative stiffness spring in the energy transfer is similar more to that of an inertial element, than to that of a conventional spring.

[Figure 17 about here.]

Fig. 18 depicts the rate of change of the total potential energy, of the kinetic energy and of the power dissipated in the damper. Similarly to Fig. 16, a phase difference of almost 180^o exists between the rate of change of the total potential energy and the one of the kinetic energy. In view of Eq. 30, this results to the activation of the damping forces and thus, a significant amount of power is absorbed in the damper.

[Figure 18 about here.]

5. Application to a periodic acoustic metamaterial lattice

In this numerical example section acoustic metamaterials are considered, in which one atom is replaced by the suggested oscillator configuration incorporating a negative stiffness element. Such metamaterials are shown to exhibit an extraordinary damping behavior, with a damping ratio to be even orders of magnitude higher than that of the original system. The concept proposed is general enough, able to lead to designs not only at a material level, but far more important, at the design of realistic engineering structures with periodic lattices, exhibiting extraordinary damping behavior, with absolutely no compromise at the structural stiffness.

The 1D wave propagation within an infinite sequence of periodic lattices with negative stiffness inclusions is hereby examined. The negative stiffness atom is used to replace the second linear oscillator (atom) used, in such a way that it retains the same static stiffness and the same damping element, however properly redesigned as per Sec. 2. The corresponding design is presented in Fig. 19.

[Figure 19 about here.]

The periodic segment, illustrated in Fig. 19 comprises a mass-in-mass configuration as in [9, 26] with the lumped mass m_2^M being included and connected to m_1^M. The κ_2^M element used to connect the two masses in [9] is hereby replaced by the suggested oscillator containing a negative stiffness element at κ_c^M. The equations of motion for the modified system are as follows

$$m_1^M \ddot{u}_1^j + c_1^M(\dot{u}_1^j - \dot{u}_1^{j-1}) - c_1^M(\dot{u}_1^{j+1} - \dot{u}_1^j) + \kappa_1^M(u_1^j - u_1^{j-1}) - \\ - \kappa_1^M(u_1^{j+1} - u_1^j) - \kappa_s^M(u_2^j - u_1^j) - \kappa_c^M(v^j - u_1^j) = 0 \tag{32a}$$

$$m_2^M \ddot{u}_2^j + \kappa_s^M(u_2^j - u_1^j) + \kappa_c^M(v^j - u_1^j) = 0 \tag{32b}$$

$$\eta^M(\dot{u}_2^j - \dot{v}^j) + \kappa_e^M(u_2^j - v^j) - \kappa_c^M(v^j - u_1^j) = 0 \tag{32c}$$

with u_1^j, u_2^j being the displacements of masses 1, 2 belonging to the jth lattice. For the infinite periodic medium Bloch's theorem [37] can be engaged in order to write a generalized relation for the displacements as

$$u_h^{j+n} = \mathrm{e}^{\mathrm{i}k(nl)+\lambda t} U_h \tag{33a}$$

$$u_h^{j-n} = \mathrm{e}^{\mathrm{i}k(-nl)+\lambda t} U_h \tag{33b}$$

$$u_h^{j} = \mathrm{e}^{\lambda t} U_h \tag{33c}$$

$$v^{j} = \mathrm{e}^{\lambda t} V \tag{33d}$$

with h=1, 2 standing for the index of the considered mass, $\pm nl$ is the total distance from the reference lattice j to the considered lattice $j \pm n$; U_h, V are the wave motion amplitudes, k represents the wavenumber and λ is a complex frequency function permitting time induced wave attenuation. In the absence of damping, $\lambda = \pm \mathrm{i}\omega$ so that the usual form of Bloch's theorem is recovered. In the presence of damping the real part of λ represents the attenuation of the wave in which case

$$\lambda_w(k) = -\xi_w(k)\omega_u(k) \pm \mathrm{i}\omega_d(k) \tag{34}$$

with ξ_w the damping ratio of the considered wave type w and ω_d the frequency at which the assumed wavenumber value for the damped wave is occurring and where the values of e_p, e_n and γ are defined as follows

$$\mathrm{e}^{\mathrm{i}kl} = e_p \tag{35a}$$

$$\mathrm{e}^{-\mathrm{i}kl} = e_n \tag{35b}$$

$$\gamma = 2(1 - e_p + e_n) = 2(1 - \cos kl) \tag{35c}$$

The system in Eq. 32 can be reformulated by considering the following state space representation

$$z_1 = U_1 \tag{36a}$$

$$z_2 = \dot{U}_1 \tag{36b}$$

$$z_3 = U_2 \tag{36c}$$

$$z_4 = \dot{U}_2 \tag{36d}$$

$$z_5 = V \tag{36e}$$

As a result, it can be cast into the following state space formulation

$$\lambda^M \begin{Bmatrix} z_1 \\ z_2 \\ z_3 \\ z_4 \\ z_5 \end{Bmatrix}^M = \begin{bmatrix} 0 & 1 & 0 & 0 & 0 \\ -\frac{\gamma\kappa_1^M + \kappa_s^M + \kappa_c^M}{m_1^M} & -\frac{\gamma c_1^M}{m_1^M} & \frac{\kappa_s^M}{m_1^M} & 0 & \frac{\kappa_c^M}{m_1^M} \\ 0 & 0 & 0 & 1 & 0 \\ \frac{\kappa_s^M + \kappa_c^M}{m_2^M} & 0 & -\frac{\kappa_s^M}{m_2^M} & 0 & \frac{\kappa_c^M}{m_2^M} \\ \frac{\kappa_c^M}{\eta^M} & 0 & \frac{\kappa_s^M}{\eta^M} & 1 & -\frac{\kappa_s^M + \kappa_c^M}{\eta^M} \end{bmatrix} \begin{Bmatrix} z_1 \\ z_2 \\ z_3 \\ z_4 \\ z_5 \end{Bmatrix}^M \tag{37}$$

The complex values of λ^M that satisfy Eq. 37 can be sought by solving the resulting eigenvalue problem

$$\lambda^M \mathbf{z}^M = \mathbf{A}^M \mathbf{z}^M \Leftrightarrow \det[\lambda^M \mathbf{I} - \mathbf{A}^M] = 0 \tag{38}$$

the solutions of which will provide the angular frequency of propagation $\omega_{d,w}$ and the damping ratio ξ_w of a certain wave

type w having a wavenumber equal to k_w and inducing structural displacements in the metamaterial lattice implied by $\mathbf{z}_w^M$.

Numerical results considering the wavenumbers as well as the damping ratios for each wave type propagating within the configuration presented in Fig. 19 will hereby be presented. For the sake of comparison, results computed for the statically equivalent structures with no negative stiffness inclusions (as presented in [9]) will also be exhibited alongside. The considered AM configuration has $\kappa_1^M = 4.182 \times 10^4$, $\kappa_2^M = \kappa_1^M/5 = 8.364 \times 10^3$, m_1^M=1 and $m_2^M = 5m_1^M$=5. The damping coefficient is chosen as η^M=1. A value for ε=3% was selected for the design of the system and a parametric survey was conducted to decide the optimal corresponding value for α=2.5 which maximizes its damping properties.

The dispersion curves of the waves propagating within the infinite waveguide are presented in Fig. 20. It can be observed that in the low frequency range the acoustic wave branches coincide for the two configurations with and without negative stiffness inclusions. The most interesting finding is the significant increase of the band-gap between the propagating waves especially in the low wavenumber range where the 'dead zone' has increased by 50% from 100 rad/sec to 150 rad/Sec. Both the acoustic and the optical wave branches seem to present a significant reduction of k for the same ω_d. This alteration is implied by a significant increase of the damping ratio as investigated below.

The structural damping ratios for each wave type as computed by the eigenvalues of Eq. 37 through Eq. 34 are exhibited in Fig. 21. A radical increase of the damping ratio can be observed for the acoustic wave branch in the region $k \in [\pi/8, \pi]$ with ξ being increased by a factor of up to 105, compared to the original system having no negative stiffness inclusions. For the optical wave the damping ratio is 25 times higher for the modified system for $\lim k \to 0^+$, while for higher values of k the optical damping ratio presents a decrease, being only 2 times greater for the modified system. Regarding the total damping ratio of the two systems a dramatic increase is observed for the system comprising negative stiffness inclusions with its ξ being increased by a factor varying between 21 and 34 for the entire wavenumber range.

[Figure 20 about here.]

6. Conclusion

The theoretical framework presented in his paper exhibits that statically and dynamically stable oscillators, incorporating negative stiffness elements can be designed. Summarising the main conclusions of the work:

(a) Once these oscillators are optimally designed according to the theory presented, they present an extraordinary damping behavior, with an apparent damping ratio to be even several orders of magnitude higher than that of the original system, especially in the cases where the original damping of the system is low.

(b) Such a design is possible, without any need for compromises in the overall stiffness of the structure. Although the elastic members of the proposed system need to be redesigned in order to present a higher stiffness than that of the original system, such an increase is kept within reasonable engineering limits.

(c) The damping element in the proposed oscillator is able to generate a phase difference between the elastic forces of the positive and the negative stiffness elements of the system. As a result, the forces either of the positive stiffness elements, or of the negative stiffness element, or both of them, are of an adequate level to balance the inertia and the excitation forces in the entire frequency range.

(d) A resonance phenomenon, although inherent and classically observed in linear SDOF systems, cannot emerge in the proposed linear oscillator.

(e) Such an oscillator concept presents the potential for numerous implementations in a large variety of technological applications, either as a discrete vibration isolator, or in the form of periodic metamaterials and composite structures. Moreover, further applications may emerge in a multiphysics environment, for instance in active vibration systems, or in electrical circuits with 'negative' capacitance elements.

References

[1] E. Rivin, Passive vibration isolation, *AS ME* Press New York, 2003.

[2] J. M. Kelly, D. Konstantinidis, Mechanics of rubber bearings for seismic and vibration isolation, John Wiley & Sons, 2011.

[3] Y. Wang, M. Ludwigson, R. Lakes, Deformation of extreme viscoelastic metals and composites, Materials Science and Engineering: A 370 (2004) 41–9.

[4] R. Lakes, Extreme damping in composite materials with a negative stiffness phase, Physical Review Letters 86 (2001) 2897–8.

[5] M. Sigalas, E. Economou, Band structure of elastic waves in two dimensional systems, Solid state communications 86 (1993) 141–3.

[6] M. S. Kushwaha, P. Halevi, L. Dobrzynski, B. Djafari-Rouhani, Acoustic band structure of periodic elastic composites, Physical Review Letters 71 (1993) 2022–3.

[7] M. Hussein, M. Leamy, M. Ruzzene, Dynamics of phononic materials and structures: Historical origins, recent progress and future outlook, Applied Mechanics Reviews, In review (2013).

[8] Z. Liu, X. Zhang, Y. Mao, Y. Zhu, Z. Yang, C. Chan, P. Sheng, Locally resonant sonic materials, Science 289 (2000) 1734–6.

[9] M. I. Hussein, M. J. Frazier, Metadamping: An emergent phenomenon in dissipative metamaterials, Journal of Sound and Vibration 332 (2013) 4767–74.

[10] K. Virk, A. Monti, T. Trehard, M. Marsh, K. Hazra, K. Boba, C. Remillat, F. Scarpa, I. Farrow, SILICOMB PEEK Kirigami cellular structures: mechanical response and energy dissipation through zero and negative stiffness, Smart Materials and Structures 22 (2013) 084014.

[11] E. Baravelli, M. Ruzzene, Internally resonating lattices for bandgap generation and low-frequency vibration control, Journal of Sound and Vibration 332 (2013) 6562–79.

[12] P. Michelis, V. Spitas, Numerical and experimental analysis of a triangular auxetic core made of CFR-PEEK using the Directionally Reinforced Integrated Single-yarn (DIRIS) architecture, Composites Science and Technology 70 (2010) 1064–71.

[13] R. Lakes, P. Rosakis, A. Ruina, Microbuckling instability in elastomeric cellular solids, Journal of Materials Science 28 (1993) 4667–72.

[14] V. Spitas, C. Spitas, P. Michelis, Modeling of the elastic damping response of a carbon nanotube–polymer nanocomposite in the stress-strain domain using an elastic energy release approach based on stick-slip, Mechanics of Advanced Materials and Structures 20 (2013) 791–800.

[15] T. Jaglinski, D. Kochmann, D. Stone, R. Lakes, Composite materials with viscoelastic stiffness greater than diamond, Science 315 (2007) 620–2.

[16] L. Dong, R. Lakes, Advanced damper with high stiffness and high hysteresis damping based on negative structural stiffness, International Journal of Solids and Structures 50 (2013) 2416–23.
[17] C. S. Wojnar, D. M. Kochmann, A negative-stiffness phase in elastic composites can produce stable extreme effective dynamic but not static stiffness, Philosophical Magazine 94 (2014) 532–55.
[18] W. Molyneaux, Supports for vibration isolation, ARC/CP-322, Aeronautical Research Council, Great Britain, 1957.
[19] D. L. Platus, Negative-stiffness-mechanism vibration isolation systems, In: SPIE's International Symposium on Optical Science, Engineering, and Instrumentation (1999) 98–105.
[20] J. Winterflood, D. Blair, B. Slagmolen, High performance vibration isolation using springs in euler column buckling mode, Physics Letters A 300 (2002) 122–30.
[21] L. Virgin, R. Davis, Vibration isolation using buckled struts, Journal of Sound and Vibration 260 (2003) 965–73.
[22] R. Plaut, J. Sidbury, L. Virgin, Analysis of buckled and pre-bent fixed-end columns used as vibration isolators, Journal of Sound and Vibration 283 (2005) 1216–28.
[23] L. Virgin, S. Santillan, R. Plaut, Vibration isolation using extreme geometric nonlinearity, Journal of Sound and Vibration 315 (2008) 721–31.
[24] R. DeSalvo, Passive, nonlinear, mechanical structures for seismic attenuation, Journal of Computational and Nonlinear Dynamics 2 (2007) 290–8.
[25] A. Carrella, M. Brennan, T. Waters, Static analysis of a passive vibration isolator with quasi-zero-stiffness characteristic, Journal of Sound and Vibration 301 (2007) 678–89.
[26] H. Huang, C. Sun, G. Huang, On the negative effective mass density in acoustic metamaterials, International Journal of Engineering Science 47 (2009) 610–7.
[27] C.-M. Lee, V. Goverdovskiy, A. Temnikov, Design of springs with negative stiffness to improve vehicle driver vibration isolation, Journal of Sound and Vibration 302 (2007) 865–74.
[28] T. D. Le, K. K. Ahn, A vibration isolation system in low frequency excitation region using negative stiffness structure for vehicle seat, Journal of Sound and Vibration 330 (2011) 6311–35.
[29] C.-M. Lee, V. Goverdovskiy, A multi-stage high-speed railroad vibration isolation system with negative stiffness, Journal of Sound and Vibration 331 (2012) 914–21.
[30] H. Iemura, M. H. Pradono, Advances in the development of pseudo-negative-stiffness dampers for seismic response control, Structural Control and Health Monitoring 16 (2009) 784–99.
[31] A. A. Sarlis, D. T. R. Pasala, M. Constantinou, A. Reinhorn, S. Nagarajaiah, D. Taylor, Negative stiffness device for seismic protection of structures, Journal of Structural Engineering 139 (2012) 1124–33.
[32] C.-M. Lee, V. Goverdovskiy, S. Samoilenko, Prediction of non-chaotic motion of the elastic system with small stiffness, Journal of Sound and Vibration 272 (2004) 643–55.
[33] A. Carrella, M. Brennan, T. Waters, V. Lopes Jr, Force and displacement transmissibility of a nonlinear isolator with high-static-low-dynamic-stiffness, International Journal of Mechanical Sciences 55 (2012) 22–9.
[34] I. Kovacic, M. J. Brennan, T. P. Waters, A study of a nonlinear vibration isolator with a quasi-zero stiffness characteristic, Journal of Sound and Vibration 315 (2008) 700–11.
[35] A. Shaw, S. Neild, D. Wagg, Dynamic analysis of high static low dynamic stiffness vibration isolation mounts, Journal of Sound Vibration 332 (2013) 1437–55.
[36] X. Huang, X. Liu, J. Sun, Z. Zhang, H. Hua, Vibration isolation characteristics of a nonlinear isolator using euler buckled beam as negative stiffness corrector: A theoretical and experimental study, Journal of Sound and Vibration 333 (2014) 1132–48.
[37] F. Bloch, Über die Quantenmechanik von Elektronen in Kristallgittern, Zeitschrift für Physik 52 (1929) 555–600.

List of Figures

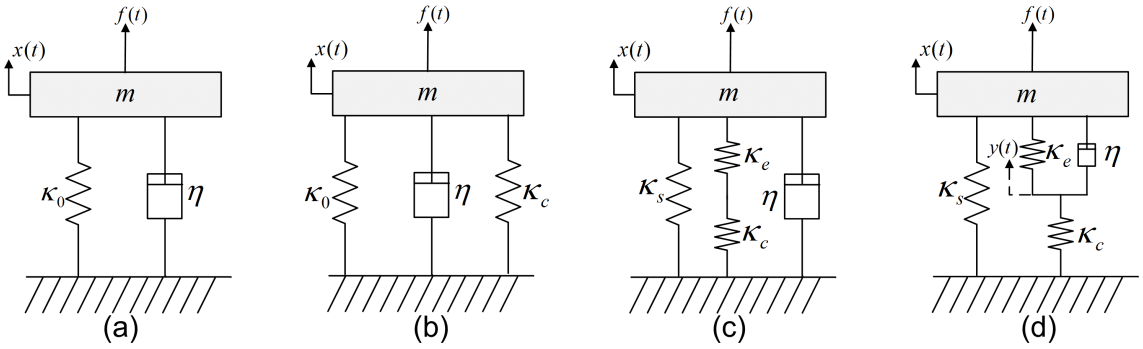

Figure 1: (a): A typical (reference) SDoF dynamic system consisting of a mass m, a stiffness κ_0 and a dashpot η. The system exhibits a natural frequency ω_0 and a damping ratio ζ_0. (b): A 'zero stiffness' oscillator. A negative stiffness element is connected in parallel to the existing stiffness element of the oscillator, in order to reduce the natural frequency. (c): A single DoF system incorporating a negative stiffness element κ_c. It is equivalent to the reference SDoF system, when the values of the stiffness elements are selected according to Eq. 1. (d): The considered linear oscillator, resulting by the reallocation of the damping element and the introduction of an internal (hidden) DOF.

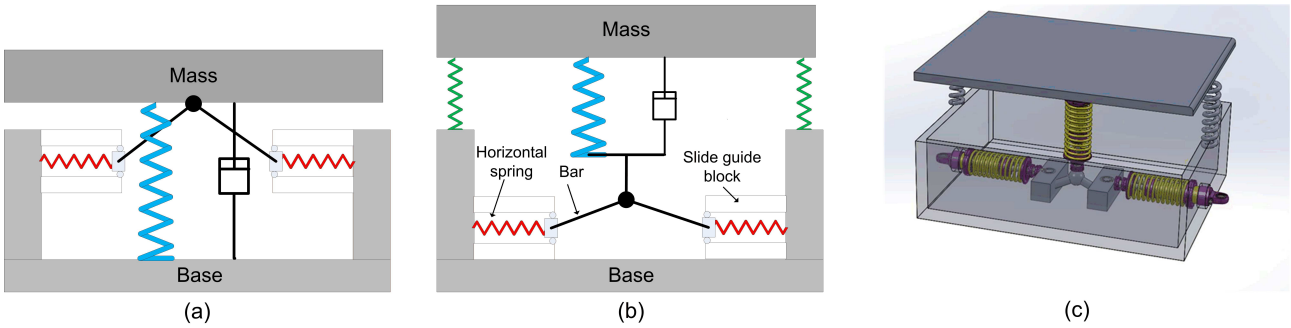

Figure 2: Realisations of negative stiffness configurations. (a): A 'zero stiffness' isolator. The 'zero stiffness' spring is realised by two horizontal springs in precompression, providing a negative stiffness in the vertical direction. (b): The considered isolator, resulting by an appropriate redistribution of the stiffness and damping elements. (c): A 3D realisation of the considered isolator.

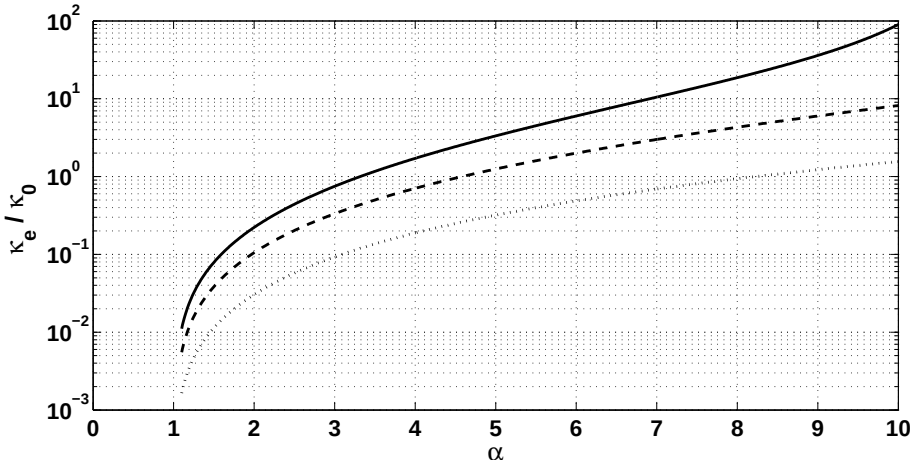

Figure 3: The relation of the ratio κ_e/κ_0 to the design parameter $\alpha = \kappa_s/\kappa_0$ in order for the considered system to retain a static equivalent stiffness κ_0 for various values of the safety margin design parameter ε: ε=1.5% ($\cdots$), ε=5% (- -), ε=10% (–). All computations conducted with ζ_0=0.01.

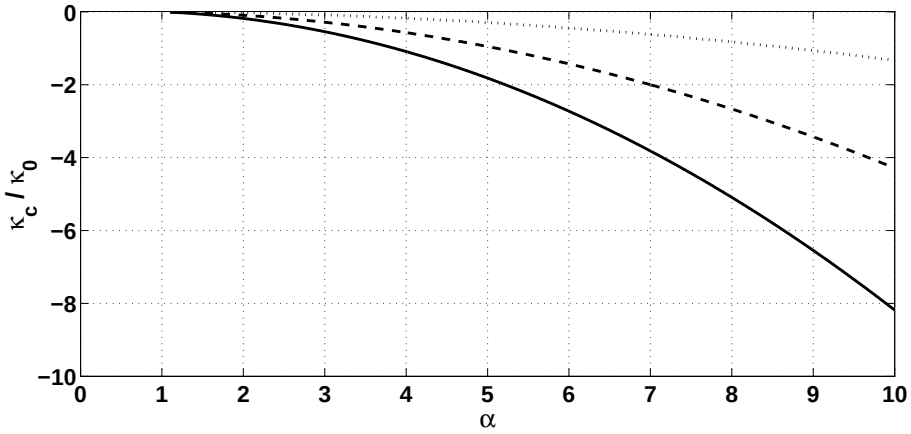

Figure 4: The relation of the ratio κ_c/κ_0 to α in order for the considered system to retain a static equivalent stiffness κ_0: ε=1.5% ($\cdots$), ε=5% (- -), ε=10% (–). All computations conducted with ζ_0=0.01.

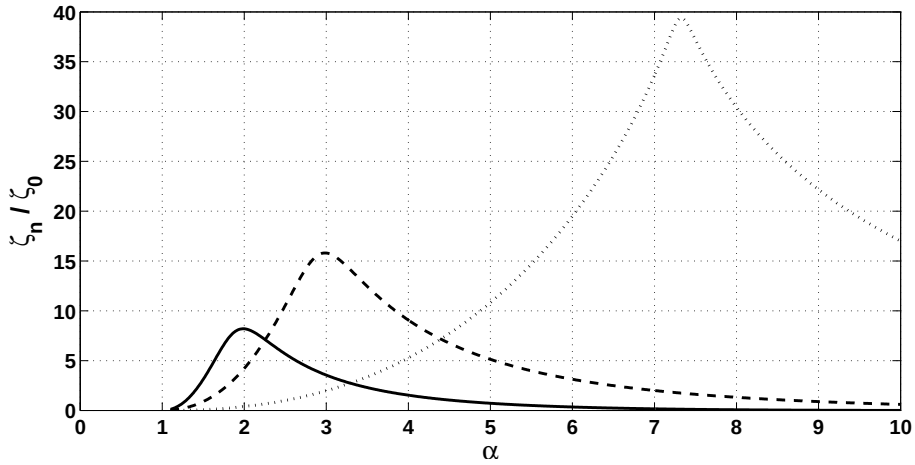

Figure 5: The impact of the ε parameter on the damping ratio enhancement ζ_n/ζ_0 of the considered system: ε=1.5% (⋯), ε=5% (- -), ε=10% (–). All computations conducted with ζ_0=0.01.

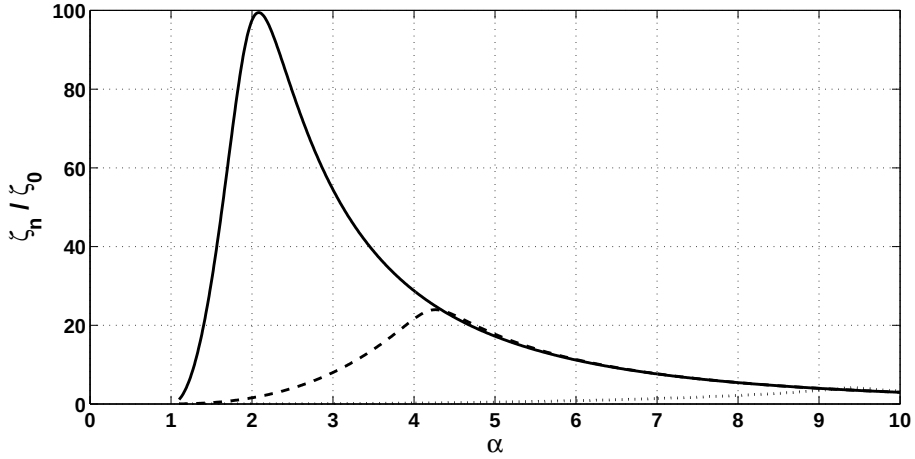

Figure 6: The impact of η on the damping ratio enhancement ζ_n/ζ_0 of the considered system: ζ_0=0.1 (⋯), ζ_0=0.01 (- -), ζ_0=0.001 (–). All computations conducted with ε=3%.

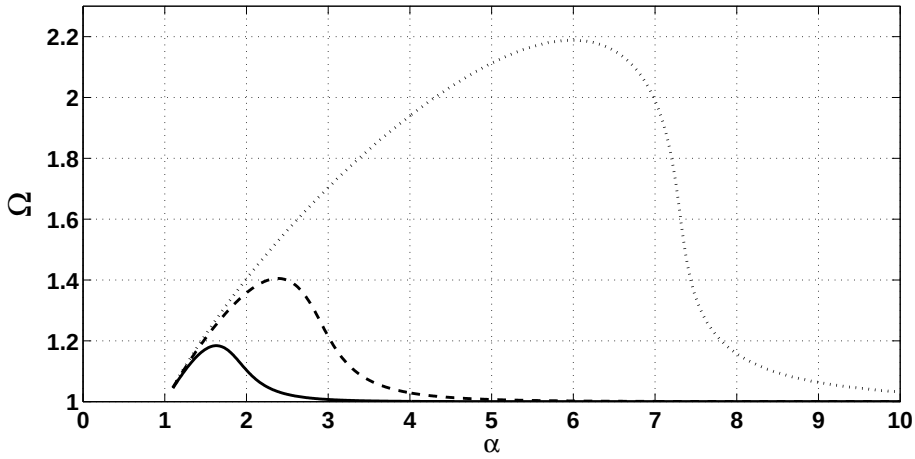

Figure 7: The impact of the ε parameter on the ratio $\Omega = \omega_n/\omega_0$ of the considered system: ε=1.5% ($\cdots$), ε=5% (- -), ε=10% (–). All computations conducted with ζ_0=0.01.

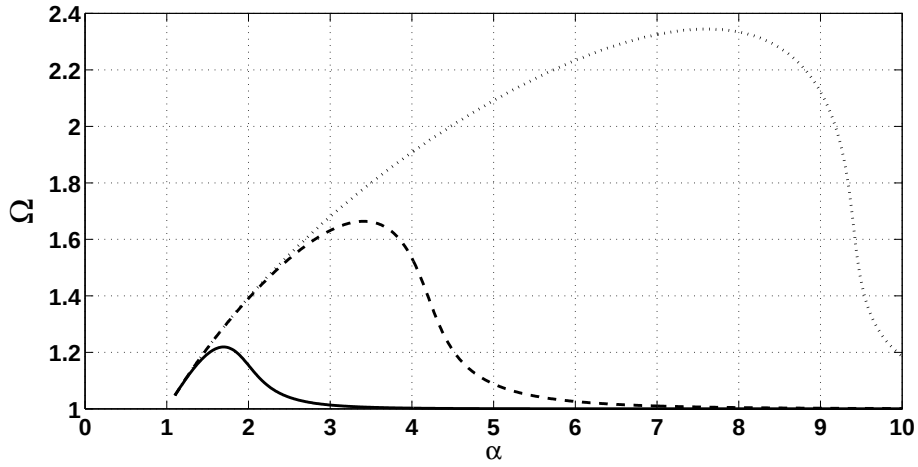

Figure 8: The impact of the damping coefficient $\eta = 2\zeta_0\sqrt{m\kappa_0}$ on the ratio $\Omega = \omega_n/\omega_0$ of the considered system: ζ_0=0.1 ($\cdots$), ζ_0=0.01 (- -), ζ_0=0.001 (–). All computations conducted with ε=3%.

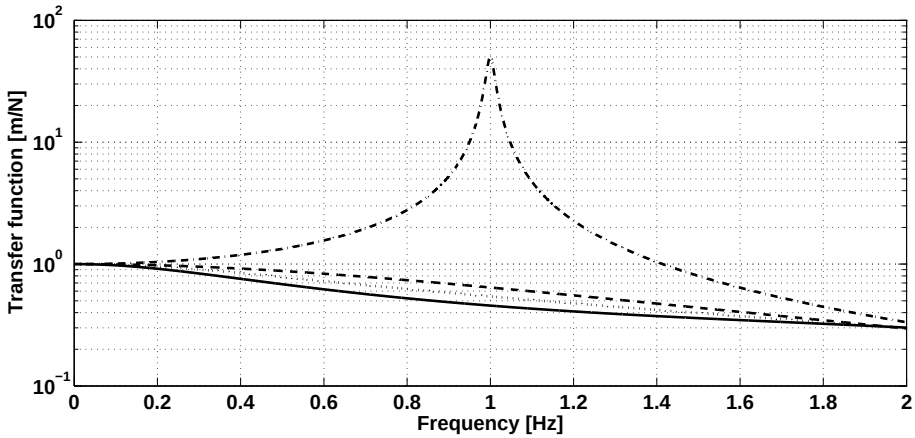

Figure 9: An attempt to minimise the displacement FRF $X(f)$ of the considered system at ω_0: i) By choosing an Ω optimal α=8.6 (–). ii) By choosing a ζ_n optimal α=10.2 (- -). i) By choosing an intermediate value α=9.4 ($\cdots$). Also exhibited the original SDoF system response (- · -). All computations conducted with ζ_0=0.01, ε=1%.

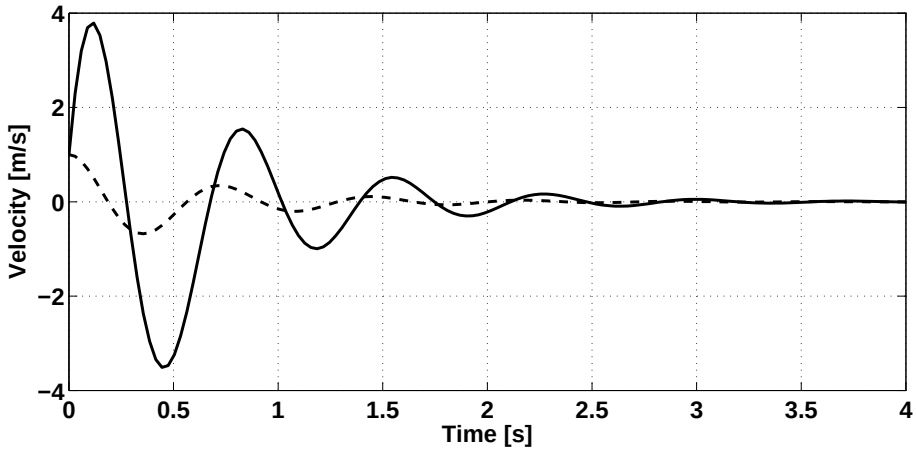

Figure 10: Time dependent velocities $\dot{x}$ and $\dot{y}$ of the modified system under a unit impulse: $\dot{y}$ (–), $\dot{x}$ (- -). All computations conducted with ε=5%, ζ_0=0.01, α=2.4 (Ω optimal)

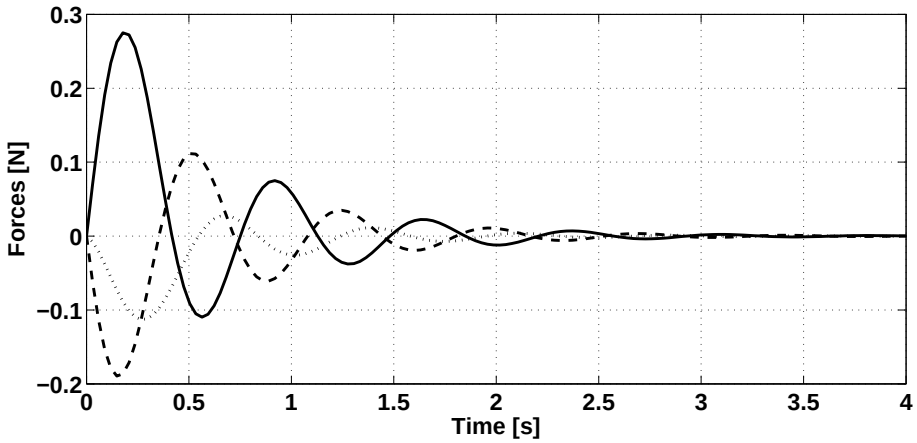

Figure 11: Time dependent forces of the modified system under a unit impulse: F_{ks} (–), F_m (- -), F_{kc} ($\cdots$). All computations conducted with ε=5%, ζ_0=0.01, α=2.4 (Ω optimal)

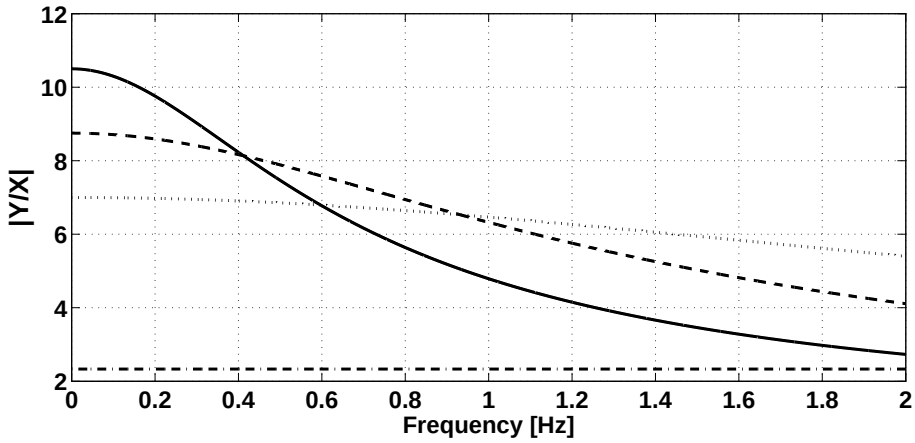

Figure 12: The magnitude of the transfer function $Y(f)/X(f)$ for the considered system: α=2 (–), α=2.4 (Ω optimal) (- -), α=3 (ζ_n optimal) ($\cdots$), α=9 (-$\cdot$-). All computations conducted with ζ_0=0.01, ε=5%.

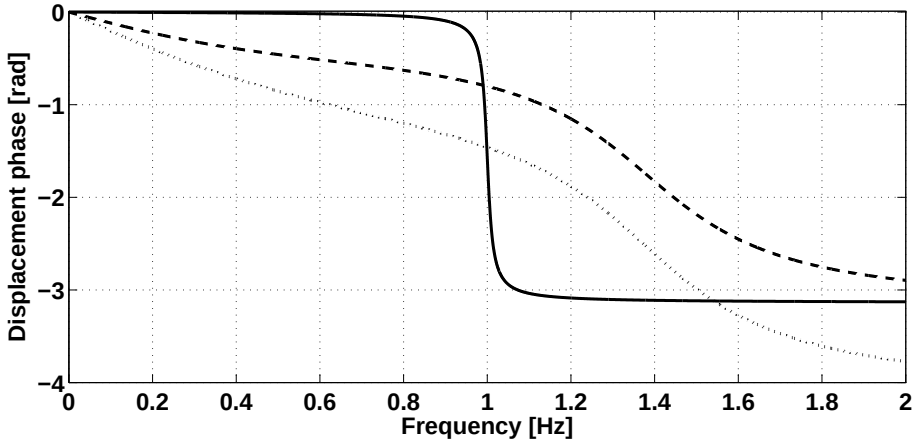

Figure 13: The phase of $X(f)$ (- -) and $Y(f)$ ($\cdots$) for α=2.4 (Ω optimal) and phase (–) of $X(f)$ for the original SDoF system. All computations conducted with ζ_0=0.01, ε=5%.

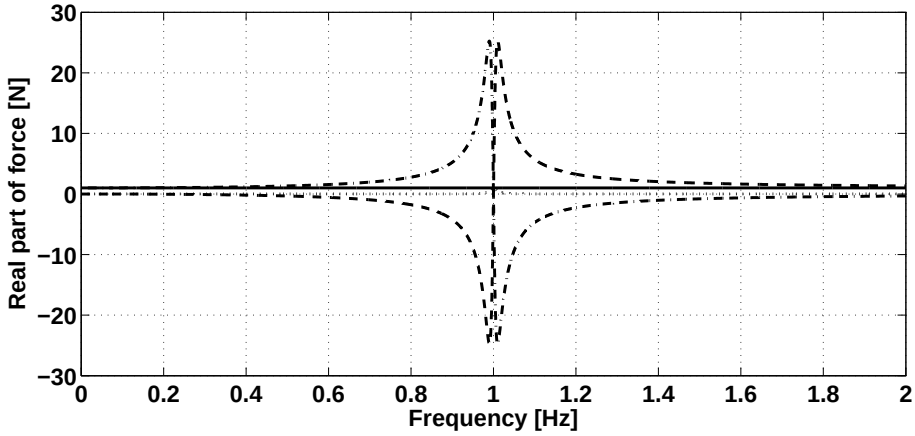

Figure 14: Real part of forces applied in the conventional SDoF system: External force f (–), Elastic force (- · -), Inertial force (- -), Damping force (· · ·). All computations conducted with α=2.4 (Ω optimal), ζ_0=0.01, ε=5%.

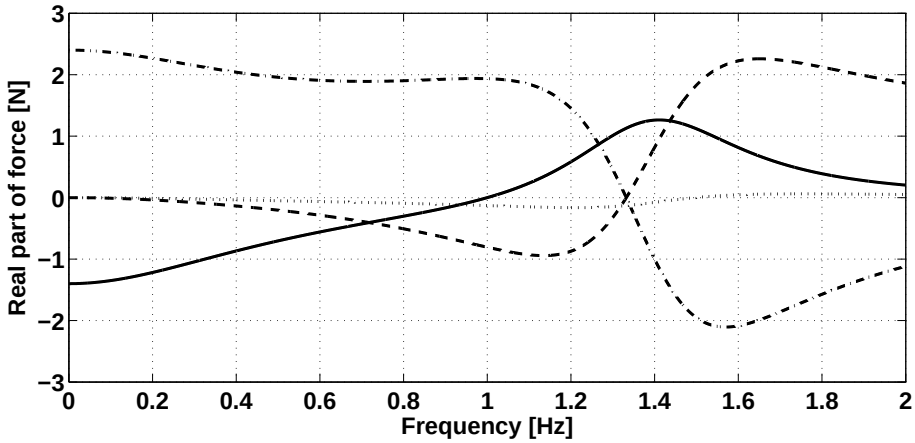

Figure 15: Real part of forces applied in the modified oscillator: Positive stiffness force F_{st} (- · -), Inertial force F_{mt} (- -), Damping force F_{ht} (· · ·), Negative stiffness force F_{ct} (–). All computations conducted with α=2.4 (Ω optimal), ζ_0=0.01, ε=5%

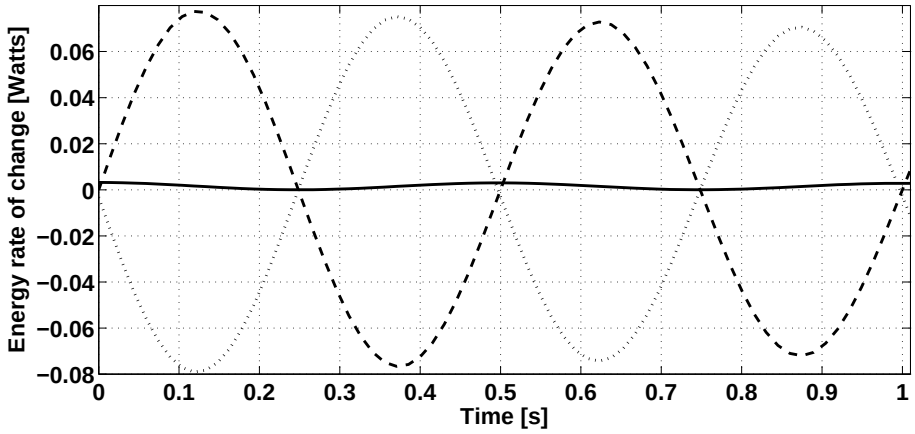

Figure 16: Rate of change of the energies within the original SDoF oscillator: Rate of change of the potential energy (- -), Rate of change of the kinetic energy (· · ·), Power dissipated in the damper (–).

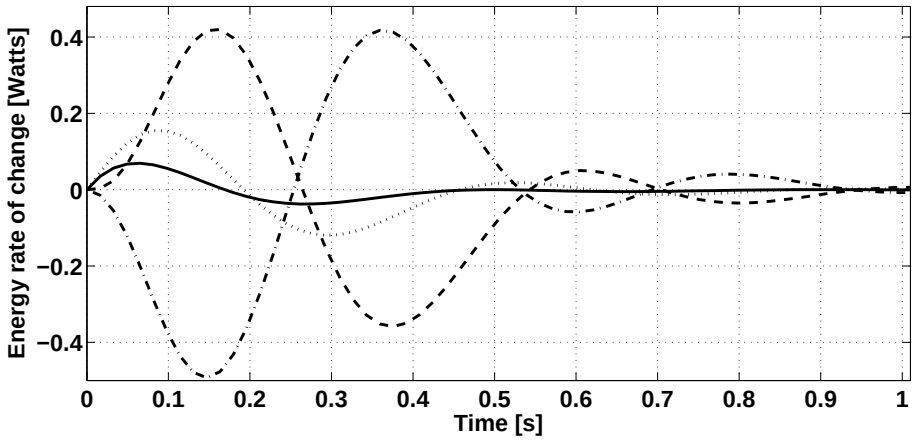

Figure 17: Rate of change of the potential energies within the suggested oscillator: Rate of change of the potential energy of κ_s ($\cdots$), Rate of change of the potential energy of κ_c (-$\cdot$-), Rate of change of the potential energy of κ_e (--), Rate of change of the total potential energy (–).

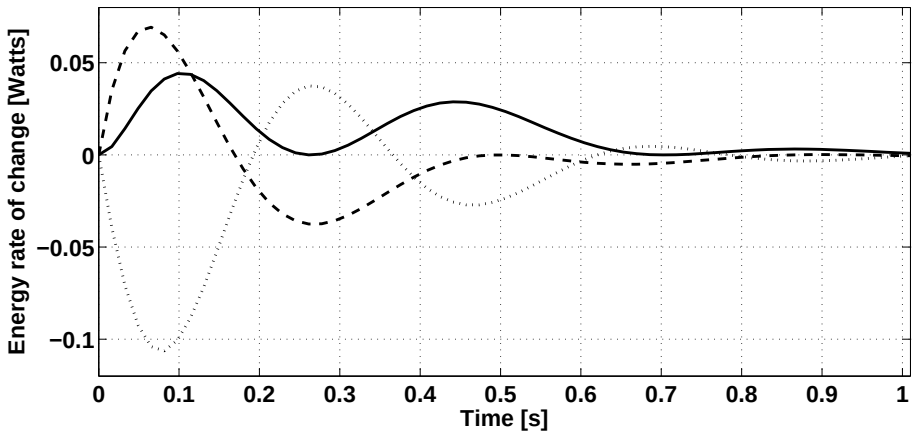

Figure 18: Rate of change of the energies within the suggested oscillator: Rate of change of the total potential energy (- -), Rate of change of the kinetic energy (· · ·), Power dissipated in the damper (–).

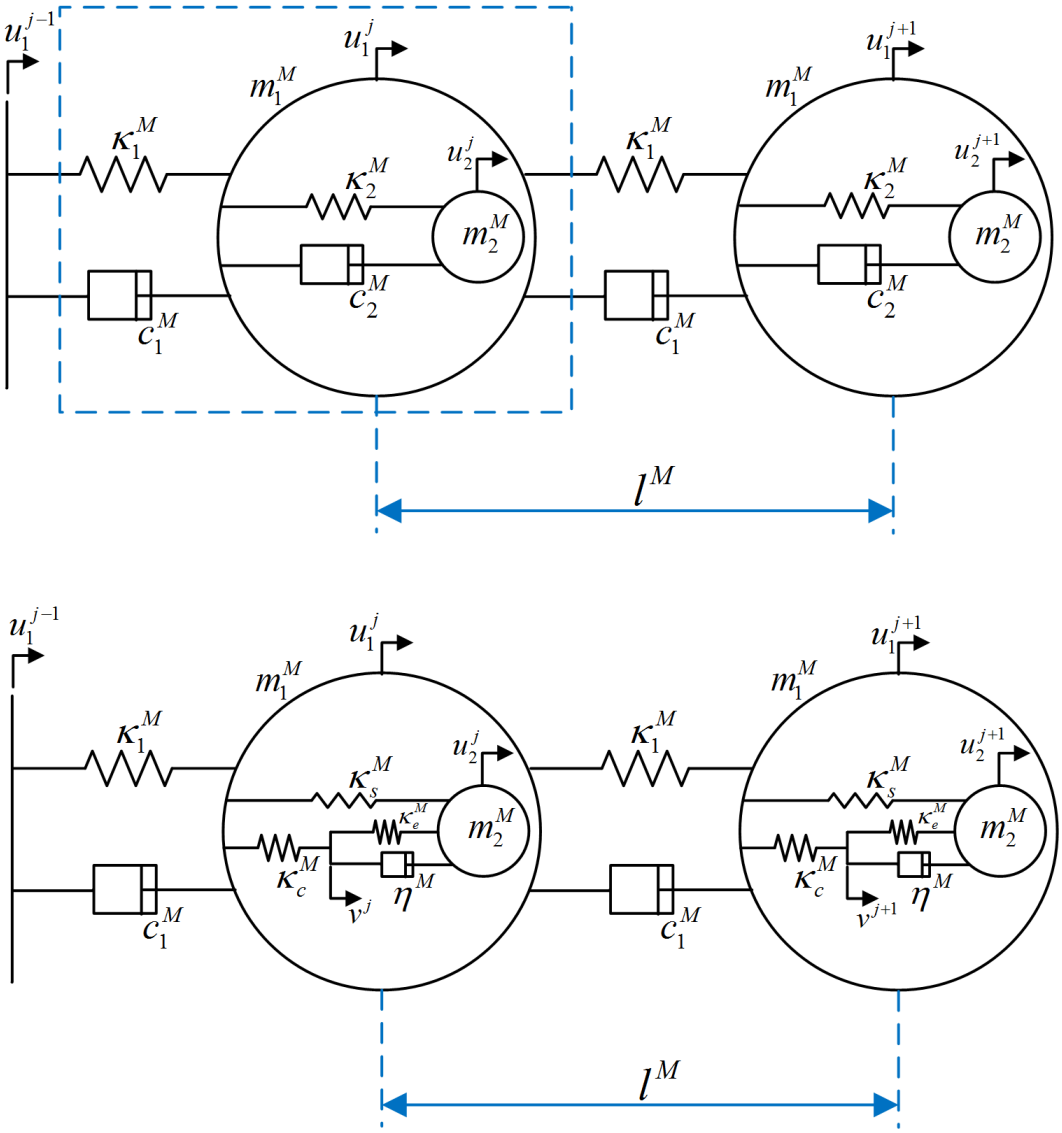

Figure 19: Left: Illustration of an Acoustic Metamaterial (M) configuration as presented in [9]. Dashed line encloses the considered periodic segment. Right: The modified Acoustic Metamaterial lattice with the second (internal) atom being replaced by a the proposed oscillator, incorporating a negative stiffness element at κ_c^M.

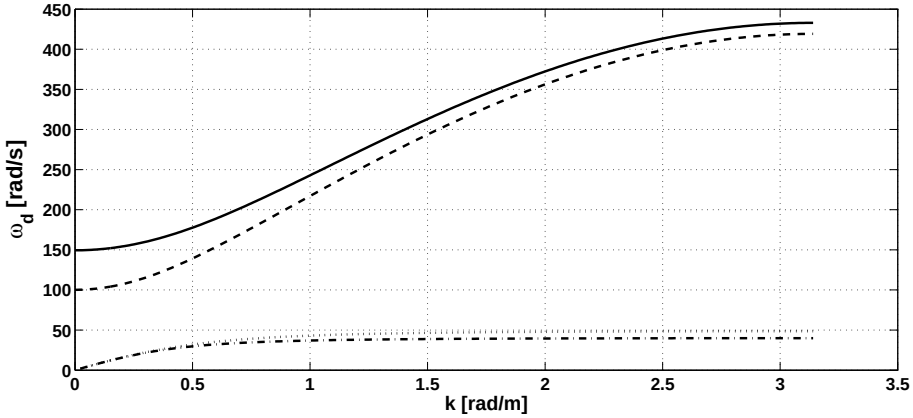

Figure 20: Wavenumber k as a function of ω_d for the acoustic wave within the acoustic metamaterial structure: Present approach with negative stiffness elements ($\cdots$), No negative stiffness inclusions (- · -). Wavenumber k as a function of ω_d for the optical propagating wave: Present approach (–), Without negative stiffness (- -). All computations conducted with α=2.5, η^M=1, ε=3%.

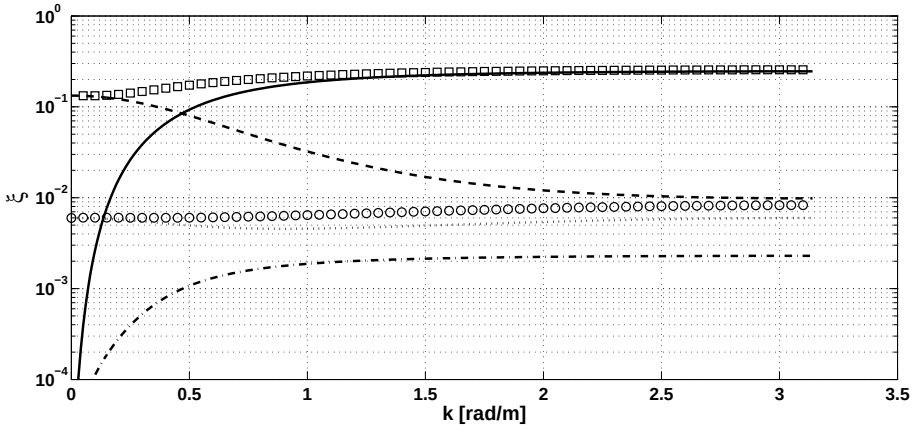

Figure 21: Damping ratio ξ as a function of k for the acoustic wave within the acoustic metamaterial structure: Present approach with negative stiffness elements (–), No negative stiffness inclusions (- · -). Damping ratio ξ as a function of k for the optical wave: Present approach (- -), Without negative stiffness ($\cdots$). Total damping ratio as a function of k: Present approach (□), Without negative stiffness (○). All computations conducted with α=2.5, η^M=1, ε=3%.